

# 1 Aeolian Sediment Supply at a Mega Nourishment

2 Bas Hoonhout<sup>a,b,\*</sup>, Sierd de Vries<sup>a</sup>

3 <sup>a</sup>*Delft University of Technology, Faculty of Civil Engineering and Geosciences,*  
4 *Department of Hydraulic Engineering, Stevinweg 1, 2628CN Delft, The Netherlands.*  
5 <sup>b</sup>*Deltares, Department of Hydraulic Engineering, Boussinesqweg 1, 2629HV Delft, The*  
6 *Netherlands.*

---

## 7 Abstract

Mega nourishments are intended to enhance growth and resilience of coastal dunes on medium to long time scales by stimulation of natural sediment transport processes. The growth and resilience of coastal dunes largely depends on the presence of a continuous supply of aeolian sediment. A recent example of a mega nourishment is the 21 Mm<sup>3</sup> mega nourishment known as the Sand Motor. The Sand Motor is intended to nourish the entire Holland coast over a period of two decades. Four years of bi-monthly topographic measurements of the Sand Motor domain provide an opportunity to analyze spatiotemporal variations in aeolian sediment supply using an aeolian sediment budget analysis. It appears that more than 58% of all aeolian sediment deposits originate from the low-lying beaches that are regularly reworked by waves. Aeolian sediment supply from higher beaches diminished after half a year after construction of the Sand Motor, likely due to the formation of deflation lag deposits that constitute a beach armor layer. The compartmentalization of the Sand Motor in armored and unarmored surfaces suggests that the construction height is an important design criterion that influences the lifetime and region of influence for any mega nourishment.

8 *Keywords:* aeolian sediment transport; aeolian sediment supply; beach  
9 armoring; sediment budgets; mega nourishment; Sand Motor

---

## 10 1. Introduction

11 In availability-limited coastal systems, the aeolian sediment transport rate  
12 is governed by the sediment availability rather than the wind transport ca-  
13 pacity. Aeolian sediment transport models typically incorporate the sediment

---

\*Corresponding author  
Preprint submitted to Coastal Management and Engineering (Bas Hoonhout),  
bas.hoonhout@deltares.nl (Bas Hoonhout) April 14, 2017

14 availability through the shear velocity threshold. However, the determina-  
15 tion of appropriate threshold values in practice appears to be challenging  
16 as the shear velocity threshold tends to vary both spatially and temporally  
17 (Barchyn et al., 2014). For example, soil moisture in the intertidal beach  
18 area fluctuates with the tidal phase and causes a local modulation of the  
19 shear velocity threshold. Moreover, a recurrence relation between sediment  
20 availability, and thus the shear velocity threshold, and sediment transport  
21 exists that complicates the a-priori determination of an appropriate thresh-  
22 old value. Consequently, aeolian sediment transport models tend to perform  
23 poorly in availability-limited systems.

24 Sherman et al. (1998) and Sherman and Li (2012) summarized the per-  
25 formance of eight aeolian sediment transport models compared to field mea-  
26 surements on a sandy beach. Although it is unknown whether this coastal  
27 system was availability-limited, all models systematically overpredicted the  
28 measured aeolian sediment transport rates. This finding is in correspondence  
29 with an abundance of coastal field studies in which aeolian sediment trans-  
30 port rates are overestimated by numerical models (e.g. Jackson and Cooper,  
31 1999; Lynch et al., 2008; Davidson-Arnott and Bauer, 2009; Aagaard, 2014).

32 In an attempt to explain the poor performance of aeolian sediment trans-  
33 port models in coastal environments, many authors emphasized the impor-  
34 tance of sediment availability and bed surface properties. Typical bed surface  
35 properties that are found along the coast and known to affect sediment avail-  
36 ability are high moisture contents (e.g. Wiggs et al., 2004; Davidson-Arnott  
37 et al., 2008; Darke and McKenna Neuman, 2008; McKenna Neuman and  
38 Sanderson, 2008; Udo et al., 2008; Bauer et al., 2009; Edwards and Namikas,  
39 2009; Namikas et al., 2010; Scheidt et al., 2010), salt crusts (e.g. Nickling and  
40 Ecclestone, 1981), vegetation (e.g. Arens, 1996; Lancaster and Baas, 1998;  
41 Okin, 2008; Li et al., 2013; Dupont et al., 2014), shell pavements (e.g. van der  
42 Wal, 1998; McKenna Neuman et al., 2012) and sorted and armored beach  
43 surfaces (e.g. Gillette and Stockton, 1989; Gillies et al., 2006; Tan et al., 2013;  
44 Cheng et al., 2015). The influence of these bed surface properties on ae-  
45olian sediment availability and transport has been investigated and typically  
46 resulted in relations between bed surface properties and the shear velocity  
47 threshold (e.g. Howard, 1977; Dyer, 1986; Belly, 1964; Johnson, 1965; Hotta  
48 et al., 1984; Nickling and Ecclestone, 1981; Arens, 1996; King et al., 2005).

49 Modeling rather than parameterization of spatiotemporal variations in  
50 aeolian sediment availability can improve coastal aeolian sediment transport  
51 estimates. As tides only affect the intertidal beach area, lag deposits and

salt crusts typically emerge from the dry beach area, and vegetation is often restricted to the dune area, sediment availability varies spatially. In addition, temporal variations in sediment availability are induced by tidal spring/neap cycles, rain showers, storm surges, seasonal variations in vegetation and progressive armoring of the beach. Due to self-grading of the sediment, progressive beach armoring creates a recurrence relation between sediment availability and transport that challenges the a-priori determination of the spatiotemporal variations in sediment availability. Process-based modeling of the instantaneous shear velocity threshold field can address these challenges and improve coastal aeolian sediment transport estimates.

This paper presents the first application of a two-dimensional (2DH) aeolian sediment availability and transport model (Hoonhout and de Vries, 2016) to hindcast the development of the sub-aerial topography of an availability-limited coastal system. The model is unique in that it describes both spatial and temporal variations in aeolian sediment availability induced by the combined influence of sediment sorting, beach armoring and soil moisture content. The influence of spatiotemporal variations in aeolian sediment availability and the model performance are illustrated by a comparison between model results and a large scale sediment budgets analysis that identifies and quantifies the main sources and sinks for aeolian sediment in the coastal system (Hoonhout and de Vries, 2017).

## 2. Field Site

The Sand Motor (or Sand Engine) is an artificial 21 Mm<sup>3</sup> sandy peninsula protruding into the North Sea off the Delfland coast in The Netherlands (Figure 1, Stive et al., 2013). The Sand Motor was constructed in 2011 and its bulged shoreline initially extended about 1 km seaward and stretched over approximately 2 km along the original coastline. The original coast was characterized by an alongshore uniform profile with a vegetated dune with an average height of 13 m and a linear beach with a 1:40 slope. The dune foot is located at a height of approximately 5 m+MSL.

Due to natural sediment dynamics the Sand Motor distributes about 1 Mm<sup>3</sup> of sand per year to the adjacent coasts (Figure 1). The majority of this sand volume is transported by tides and waves. However, the Sand Motor is constructed up to 5 m+MSL and locally up to 7 m+MSL, which is in either case well above the maximum surge level of 3 m+MSL (Figure 2c). Therefore, the majority of the Sand Motor area is uniquely shaped by wind.

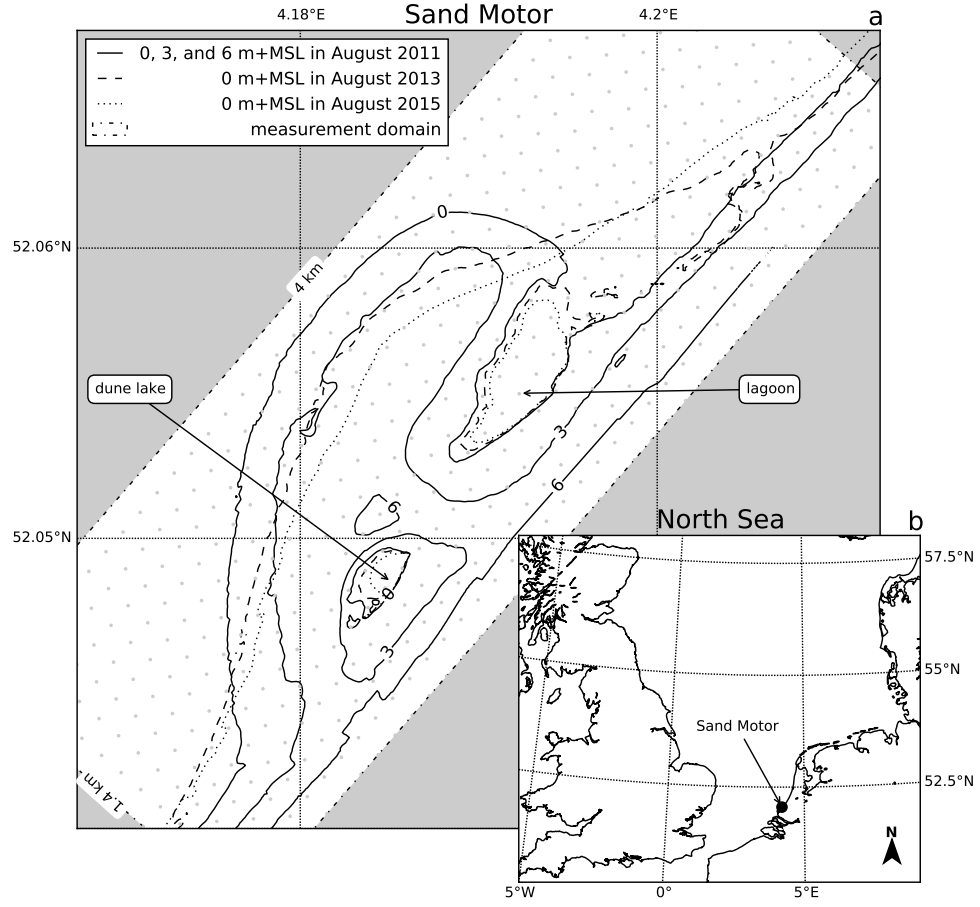


Figure 1: Location, orientation, appearance and evolution of the Sand Motor between construction in 2011 and 2015. The box indicates the measurement domain used in the remainder of this paper. A 100 x 100 m grid aligned with the measurement domain is plotted in gray as reference.

The Sand Motor comprises both a dune lake and a lagoon that act as large traps for aeolian sediment (Figure 1). The lagoon is affected by tidal forcing, although the tidal amplitude quickly diminished over time as the entry channel elongated. The tidal range of about 2 m that is present at the Sand Motor periphery (Figure 2c), is nowadays damped to less than 20 cm inside the lagoon (de Vries et al., 2015). Consequently, the tidal currents at the closed end of the lagoon, where most aeolian sediment is trapped, are negligible.

The dominant wind direction at the Sand Motor is south to southwest (Figure 2a). However, during storm conditions the wind direction tends to be southwest to northwest. During extreme storm conditions the wind direction tends to be northwest. Northwesterly storms are typically accompanied by significant surges as the fetch is virtually unbounded to the northwest, while surges from the southwest are limited due to the presence of the narrowing of the North Sea at the Strait of Dover (Figure 1, inset).

### 3. Model approach

A two-dimensional (2DH) model of the Sand Motor that includes limitations in sediment availability is constructed and calibrated based on four years of field measurements on wind, tides, waves and topography. The calibrated model is used to investigate the influence of spatiotemporal variations in aeolian sediment availability on sediment accumulation in the Sand Motor domain.

To test that the Sand Motor mega nourishment is indeed an availability-limited coastal system, the measured long-term sediment accumulation volumes (Hoonhout and de Vries, 2017) are first compared to a reference model that assumes no limitations in sediment availability exist.

#### 3.1. Reference model

A selection of equilibrium sediment transport formulations is used as reference model. An equilibrium sediment transport formulation describes the wind transport capacity in given conditions. In conjunction with a shear velocity threshold based on only a constant uniform median grain size, an estimate of the potential aeolian sediment accumulation in absence of availability-limitations can be obtained. The potential aeolian sediment accumulation or cumulative wind transport capacity  $Q$  [m<sup>3</sup>] in the Sand Motor domain is estimated based on hourly averaged time series of the wind speed

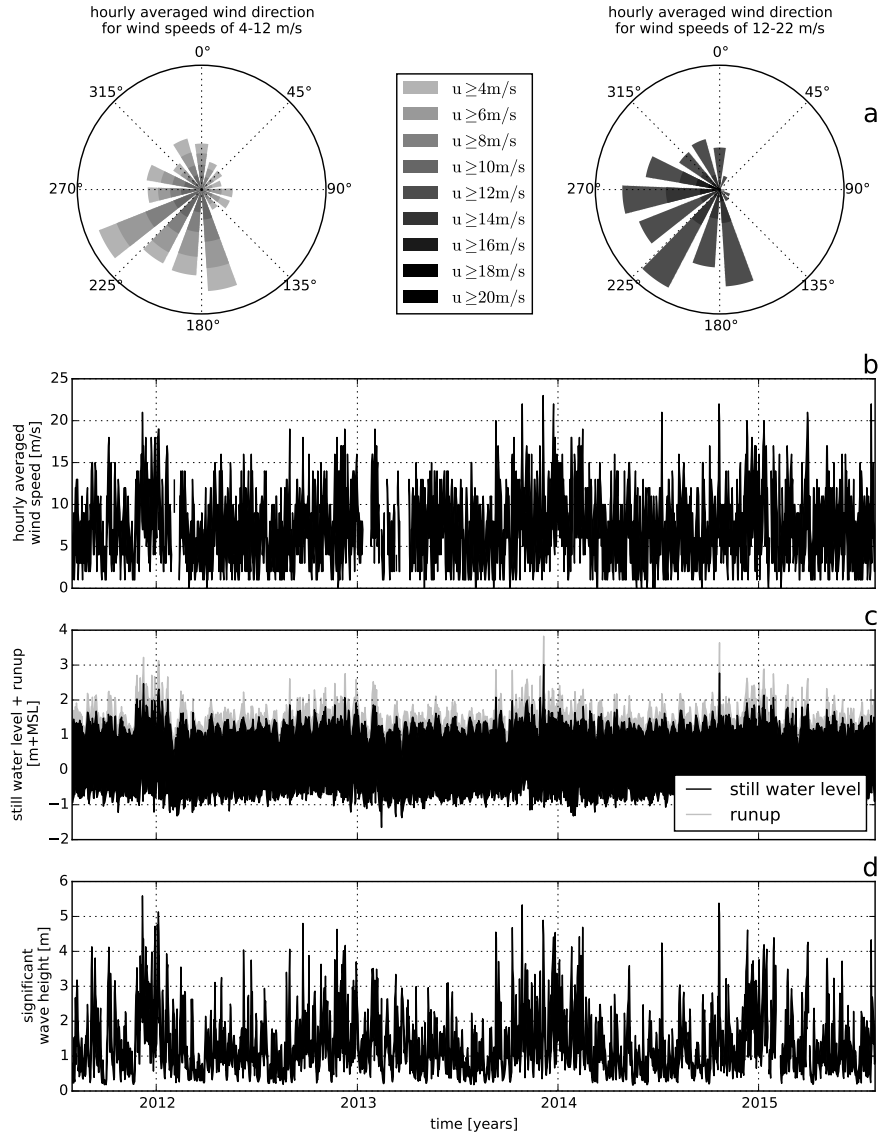


Figure 2: Wind and hydrodynamic time series from 2011 to 2015. Hourly averaged wind speeds and directions are obtained from the KNMI meteorological station in Hoek van Holland (upper panels). Offshore still water levels, wave heights and wave periods are obtained from the Europlatform (lower panels). Runup levels are estimated following Stockdon et al. (2006).

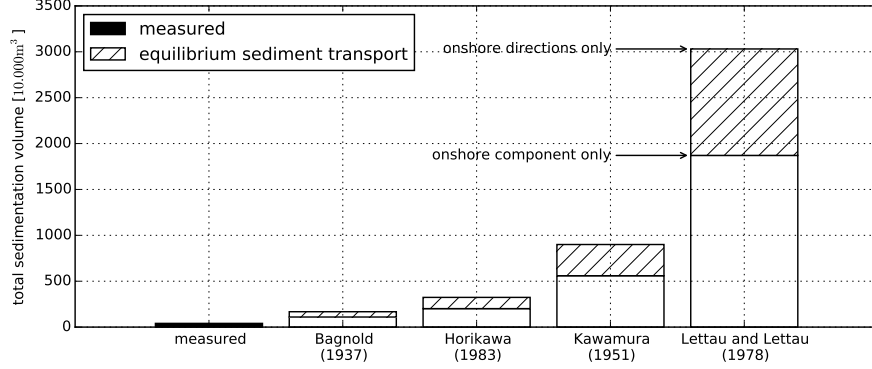


Figure 3: Comparison of the cumulative wind transport capacity according to a selection of equilibrium sediment transport formulations and measured total sedimentation in the Sand Motor domain. The equilibrium sediment transport is based on an hourly averaged wind speed and direction time series from September 1, 2011 until September 1, 2015. Offshore wind directions are discarded. For the upper boundary of each estimate all wind directions are weighted equally. For the lower boundary of each estimate the wind directions are weighted according to the magnitude of the onshore component.

123  $u_z$  [m/s] and direction  $\theta_u$  [°] obtained from the KNMI meteorological station  
 124 in Hoek van Holland following:

$$Q = \sum q \cdot \frac{\Delta t \cdot \Delta y}{(1 - p) \cdot \rho_p} \cdot f_{\theta_u} \quad (1)$$

125 where the temporal resolution  $\Delta t = 1$  h, the alongshore span of the domain  
 126  $\Delta y = 4$  km, the porosity  $p = 0.4$ , the particle density  $\rho_p = 2650$  kg/m<sup>3</sup>,  
 127 the sediment transport rate  $q$  is given by the equilibrium sediment transport  
 128 formulation (Table 1) and  $f_{\theta_u}$  is a factor to account for the wind direction.  
 129 The wind direction can be accounted for by only including the onshore wind  
 130 component with respect to the original coastline orientation. However, given  
 131 the typical Sand Motor geometry (Figure 1), sediment is likely to be trapped  
 132 in the dune lake and lagoon even with alongshore wind. Therefore it can  
 133 be assumed that the onshore wind component will provide a lower limit of  
 134 the cumulative wind transport capacity. Similarly, an upper limit can be  
 135 obtained by assuming that all onshore wind directions contribute equally to  
 136 the cumulative wind transport capacity. For the upper limit the factor  $f_{\theta_u}$   
 137 is defined as:

$$f_{\theta_u} = \begin{cases} 1 & \text{if } \cos(312^\circ - \theta_u) \geq 0 \\ 0 & \text{if } \cos(312^\circ - \theta_u) < 0 \end{cases} \quad (2)$$

138 while for the lower limit the factor  $f_{\theta_u}$  is defined as:

$$f_{\theta_u} = \max(0 ; \cos(312^\circ - \theta_u)) \quad (3)$$

139 where  $312^\circ$  accounts for orientation of the original coastline. Figure 3 presents  
 140 an overview of the cumulative wind transport capacity in the Sand Motor  
 141 domain over the period between September 1, 2011 and September 1, 2015  
 142 according to a selection of equilibrium sediment transport formulations and  
 143 in comparison with the measured accumulation volumes. The estimates of  
 144 the wind transport capacity show a large variation between formulations that  
 145 are mainly due to the incorporation of the shear velocity threshold. How-  
 146 ever, all formulations overestimate the measured sediment accumulation in  
 147 the Sand Motor domain with at least a factor 3 – 4. The large variation and  
 148 consistent overestimation is in accordance with the review of aeolian sedi-  
 149 ment transport models presented by Sherman and Li (2012). The consistent  
 150 overestimation of the measured sedimentation volumes in the Sand Motor  
 151 domain suggest that the Sand Motor is indeed an availability-limited coastal  
 152 system.

### 153 3.2. Schematization

154 A two-dimensional (2DH) aeolian sediment availability and transport  
 155 model for the Sand Motor mega nourishment is constructed for the four years  
 156 between September 1, 2011 and September 1, 2015, which is shortly after the  
 157 nourishment was placed. The model’s topography and grid are based on the  
 158 measured topographies of August 3, 2011 and later. The topographies are  
 159 rotated  $48^\circ$  and interpolated to a 50 x 50 m grid spanning 1.5 km cross-shore  
 160 and 4 km alongshore with respect to the original coastline, not including the  
 161 dunes (Figure 4, upper panel).

162 Four years of hourly wind speed and direction data measured at 10 m  
 163 above the bed is obtained from the KNMI meteorological station at Hoek  
 164 van Holland (Figure 2a,b). Hourly offshore water levels and wave heights are  
 165 obtained from the Europlatform for the same period (Figure 2c,d).

166 An average lognormal grain size distribution with a median diameter  
 167  $d_{50} = 335 \mu\text{m}$  is used as measured at the Sand Motor field site. The sand  
 168 fractions cover a range from 0.1 to 2 mm. The amount of shells and other



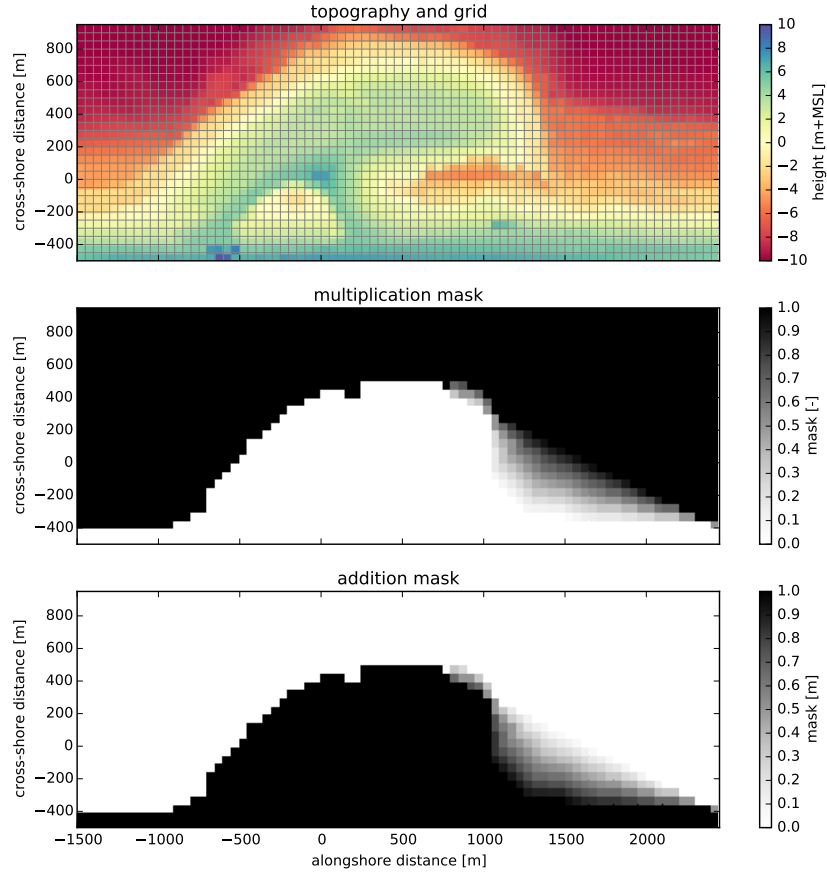


Figure 4: Model grid and topography based on the topographic survey of August 3, 2011 (upper panel) and hydrodynamic mask used to limit tidal and wave motions in the dune lake and lagoon (middle and lower panels). Water levels and wave heights are uniformly imposed to the model and multiplied by the multiplication mask and subsequently increased with the addition mask.

Table 1: Equilibrium sediment transport formulations, coefficient values\* and the ratio between measurements and model results.

Reference	Equation	$C$	Ratio
Bagnold (1937)	$q = C \frac{\rho_a}{g} \sqrt{\frac{d_n}{D_n}} (u_* - u_{*th})^3$	1.8	3 – 4
Horikawa et al. (1983)	$2^* q = C \frac{\rho_a}{g} (u_* + u_{*th})^2 (u_* - u_{*th})$	1.0	5 – 8
Kawamura (1951)		2.78	14 – 22
Lettau and Lettau (1978)	$q = C \frac{\rho_a}{g} \sqrt{\frac{d_n}{D_n}} (u_* - u_{*th}) u_*^2$	6.7	46 – 75

\* Other values are the shear velocity  $u_* = \alpha \cdot u_z$  m/s, the shear velocity threshold  $u_{*th} = \alpha \cdot 3.87$  m/s, the conversion factor from free-flow wind velocity to shear velocity  $\alpha = 0.058$ , the air density  $\rho_a = 1.25$  kg/m<sup>3</sup>, the particle density  $\rho_p = 2650.0$  kg/m<sup>3</sup>, the gravitational constant  $g = 9.81$  m/s<sup>2</sup>, the nominal grain size  $d_n = 335$   $\mu$ m, a reference grain size  $D_n = 250$   $\mu$ m and the height above the bed of the wind measurement  $z = 10$  m.

roughness elements in the originally nourished sand is estimated to be 5%. The estimate is based on three sediment samples obtained from the field site 0.5 m below the bed surface. Additional fractions ranging from 2 to 32 mm are added according to a lognormal distribution to account for the presence of roughness elements in the bed. The grain size distribution is used to populate the initial bed that consists of 10 bed composition layers with a thickness of 1 cm each.

The hindcast aims at the large scale and long term sedimentation volumes as presented by Hoonhout and de Vries (2017). Therefore an efficient, but diffusive, implicit Euler Backward scheme with a timestep of 1 h is used that does not resolve high frequency variations in wind or sediment transport. Consequently, the model produces smooth solutions that describe hourly steady states based on the instantaneous average wind speed and sediment availability.

Bagnold (1937) is selected as equilibrium sediment transport formulation as it is derived separately for different grain sizes and therefore suitable for multi-fraction aeolian sediment transport. Alternative formulations (Table 1) are derived for wider grain size distributions that do not necessarily result in a monotonic relation between the grain size and the sediment transport rate (e.g. Kawamura, 1951; Horikawa et al., 1983). Such non-monotonic relation is unrealistic in a multi-fraction context as it would result in a preference to transport both fine sediment and large elements that are considered non-

erodible. Moreover, the formulation of Bagnold (1937) overestimates the measured aeolian sediment transport rates in the Sand Motor domain less compared to alternative formulations (Table 1, rightmost column).

Water levels and wave heights are initially uniformly imposed to the model. Consequently, the tidal range, mean water level and wave heights that are present at the Sand Motor periphery are also present in the dune lake and lagoon. In reality the tidal range and wave heights in the dune lake and lagoon are much lower, while the mean water level in the dune lake and lagoon is elevated compared to mean sea level (de Vries et al., 2015). To account for these spatial differences in hydrodynamics a hydrodynamic mask is applied (Figure 4, middle and lower panel; Appendix ??)

Subtidal changes in topography are not simulated by the model. The subtidal changes can be important to aeolian sediment transport as the location and size of aeolian sediment erosion and deposition areas might change. To account for these changes, measured topographies are imposed to the model through a Basic Model Interface (BMI, Peckham et al., 2013, Appendix ??).

All measured topographies in the period between September 1, 2011 and September 1, 2015 are linearly interpolated in time as to obtain daily updates of the Sand Motor’s topography. The hydrodynamic mask is updated along with the topography. The presented aeolian sediment transport rates are based on the time-integrated entrainment and deposition rates that are computed by the model rather than differences in topography.

### 3.3. Calibration

The model is calibrated on the shape of roughness elements that emerge from the bed and shelter the sand surface from wind erosion, the drying rate of the soil and the time needed for the sediment transport to adapt to changing wind conditions. These processes are represented in the model by parameters for which data or literature can only provide approximate values:

1.  $\sigma$ , as used in the formulation of Raupach et al. (1993, Equation ??), is the ratio between the basal and frontal area of the roughness elements that constitute the beach armor layer.
2.  $T_{\text{dry}}$  is the time scale at which the beach dries out after flooding (Equation ??). It represents the time in which the soil moisture content halves in case the beach is not inundated and no evaporation occurs.
3.  $T$  is the adaptation time scale in the right-hand side of the advection equation (Equation ??). It represents the time scale to which

the sediment transport adapts to variations in the wind conditions and sediment availability.

The implementation of roughness elements is characterized by three calibration parameters:  $m$ ,  $\beta$  and  $\sigma$  (Equation ??).  $m$  is a factor to account for the difference between the mean and maximum shear stress and is usually chosen as 0.5 for field applications (Raupach et al., 1993; McKenna Neuman et al., 2012). Numerically it is irrelevant if  $\beta$  or  $\sigma$  is calibrated as they only appear as a ratio  $\frac{\beta}{\sigma}$  in the model implementation. As  $\beta$  is the ratio between the drag coefficient of the roughness elements alone and the drag coefficient of the unarmored sandy bed, the value can be assumed to be reasonably generic. In contrast,  $\sigma$  depends on the shape and protrusion of the roughness elements and therefore depends on the field site and varies in time. For example, a spherical object placed on top of the bed would be represented by  $\sigma = 1$ , while a spherical object protruding halfway through the bed (hemisphere) would be represented by  $\sigma = 2$ . Consequently, calibration of  $\sigma$  seems to be preferable as it is less certain. Wind tunnel experiments presented by McKenna Neuman et al. (2012) investigated the influence of a lag deposits, consisting of shells and shell fragments, on aeolian sediment transport. Values for the calibration coefficients  $m$  and  $\beta$  were found to be 0.5 and 130 respectively and are adopted for the Sand Motor hindcast. An optimal average value for  $\sigma$  is obtained by systematic variation between 2 and 20.

The drying rate of the beach ( $T_{\text{dry}}$ ) depends on many factors, like grain size, soil moisture content, groundwater level, wind speed and solar radiation. The use of a single time scale as aggregate for these processes is an oversimplification of reality. Therefore a wide range of parameter values is covered in the calibration.  $T_{\text{dry}}$  is varied between 0.1 and 10 hours where the former results in virtually instant drying and the latter results in an intertidal beach that is permanently too moist for aeolian sediment transport to be initiated.

The adaptation time scale ( $T$ ), that represents the swiftness of aeolian sediment transport to adapt to changing wind conditions, is in the order of seconds (Davidson-Arnott et al., 2008; de Vries et al., 2014). As the model time step is orders of magnitude larger, the model effectively solves steady states and the value for  $T$  will not affect temporal variations in sediment transport. However, the adaptation time scale also affects the development of the saltation cascade in space. Sediment transport increases in downwind

264 direction from a zero-flux boundary, like the water line in case of onshore  
 265 wind, with a rate that is governed by the value of  $T$ . Consequently,  $T$  influ-  
 266 ences the width of the source area in case of abundant sediment availability.  
 267  $T$  is varied between 1 and 10 seconds.

268 The calibration is performed based on the bi-monthly erosion and de-  
 269 position volumes as measured in the Sand Motor domain (Hoonhout and  
 270 de Vries, 2017). The erosion and deposition volumes are determined within  
 271 seven predefined zones (Figure 5) that aim to separate areas with marine  
 272 influences from areas without marine influences, and separate areas with net  
 273 aeolian erosion from areas with net aeolian deposition. The zonation is based  
 274 on the 0, 3 and 5 m+MSL contour lines that roughly correspond with the  
 275 mean water level, maximum runup level or berm edge and the dune foot  
 276 respectively. The average  $R^2$  value of the time series for erosion and deposi-  
 277 tion is used as benchmark. The  $R^2$  value represents the fraction of explained  
 278 variance and is defined as:

$$R^2 = \frac{\sum_n [V_{\text{measured}}^n - V_{\text{model}}^n]^2}{\sum_n [V_{\text{measured}}^n - \overline{V_{\text{measured}}^n}]^2} \quad (4)$$

279 where  $V^n$  is the measured or modeled sediment volume in time period  $n$ .  
 280 The overbar denotes time-averaging. In addition the root-mean-square error  
 281 (RMSE) is presented as absolute measure for the model accuracy, which is  
 282 defined as:

$$RMSE = \sqrt{\sum_n [V_{\text{measured}}^n - V_{\text{model}}^n]^2} \quad (5)$$

283 The calibration itself is performed in three steps:

- 284 1. A coarse calibration on  $\sigma$  and  $T_{\text{dry}}$ .
- 285 2. A calibration on  $T$  using the provisional optimal settings for  $\sigma$  and  $T_{\text{dry}}$ .
- 286 3. A fine calibration on  $\sigma$  and  $T_{\text{dry}}$  using the optimal setting for  $T$ .

## 287 4. Results

288 The optimal model settings were chosen from 150 realizations (Figure 6).  
 289 The optimal realization has an  $R^2$  value of 0.93 and a RMSE of  $3 \cdot 10^4 \text{ m}^3$ . The  
 290 corresponding optimal parameter settings are found to be  $\sigma = 9.2$ ,  $T_{\text{dry}} = 2$   
 291 h and  $T = 1$  s. These settings were ultimately selected from a cluster of

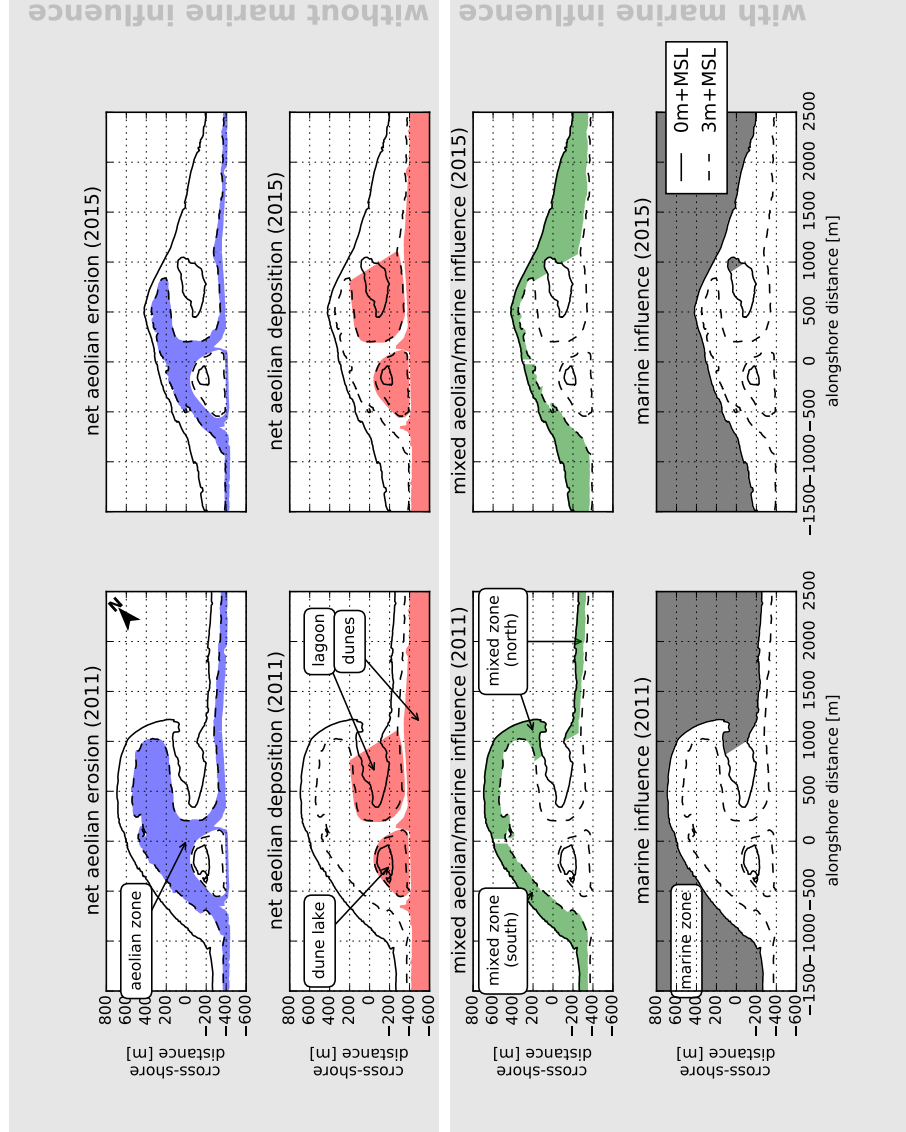


Figure 5: Zonation of the Sand Motor domain into zones with net aeolian erosion and no marine influence, net aeolian deposition and no marine influence, mixed aeolian/marine influence and marine influence. Zonation is based on the 0, 3 and 5 m+MSL contour lines that roughly correspond with the mean water level, maximum runup level or berm edge and the dune foot respectively. Left panels: 2011. Right panels: 2015. Source: Hoonhout and de Vries (2017).

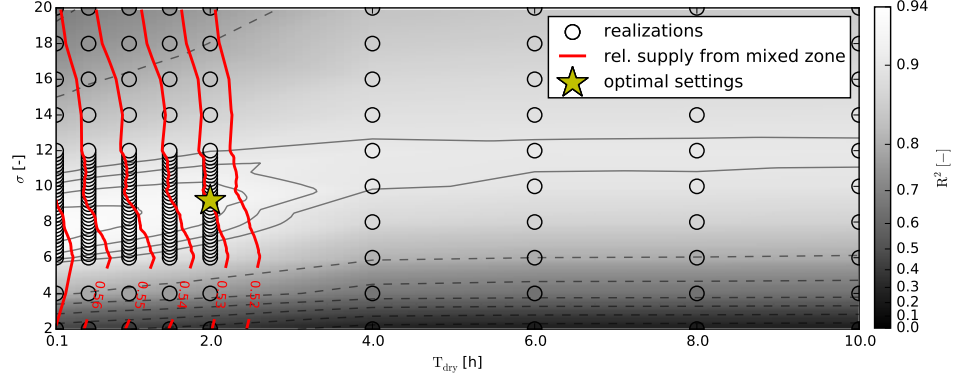


Figure 6: Systematic variation of calibration parameters  $\sigma$  and  $T_{\text{dry}}$  with  $T = 1$  s. The circles indicate the realizations made. The colored background depicts a linear interpolation of the  $R^2$  values with respect to the data presented in Figure ???. The solid isolines depict  $R^2$  values from 0.90 to 0.93, while the dashed isolines depict  $R^2$  values from 0.0 to 0.9. The red lines depict the relative supply from the mixed zones ranging from 52% to 57%. The yellow star indicates the optimal value model settings.

292 realizations with comparable  $R^2$  values based on the relative sediment supply  
 293 from the mixed zones (Figure 5, third row) at the end of the simulation. An  
 294 overview of all model settings for the calibrated model is given in Appendix  
 295 ??.

296 Figure 7 shows that erosion from the aeolian zone (Figure 5, first row) is  
 297 most pronounced in the first year and least in the second year in both the  
 298 measurements and the model results. Also the deposition of aeolian sediment  
 299 in the dune lake and lagoon (Figure 5, second row) is observed in both  
 300 the measurements and model results, although the model underestimates  
 301 these deposited volumes. The deposition in the dune lake and lagoon is also  
 302 more localized in the measurements than in the model results. The spatial  
 303 variability in the erosion of the aeolian zone is larger in the measurements  
 304 than in the model results. The large variability measured in the mixed zone  
 305 is not present in the model results as hydrodynamic sediment transport is  
 306 not simulated.

307 The development of the total erosion and deposition volumes in the Sand  
 308 Motor domain in the four year period is represented well by the model (Figure  
 309 8). The dune accumulation volume is overestimated at the expense of the  
 310 sediment volumes deposited in the dune lake and lagoon (Figure 9). As  
 311 the dune area is not included in the model domain, the sediment flux over

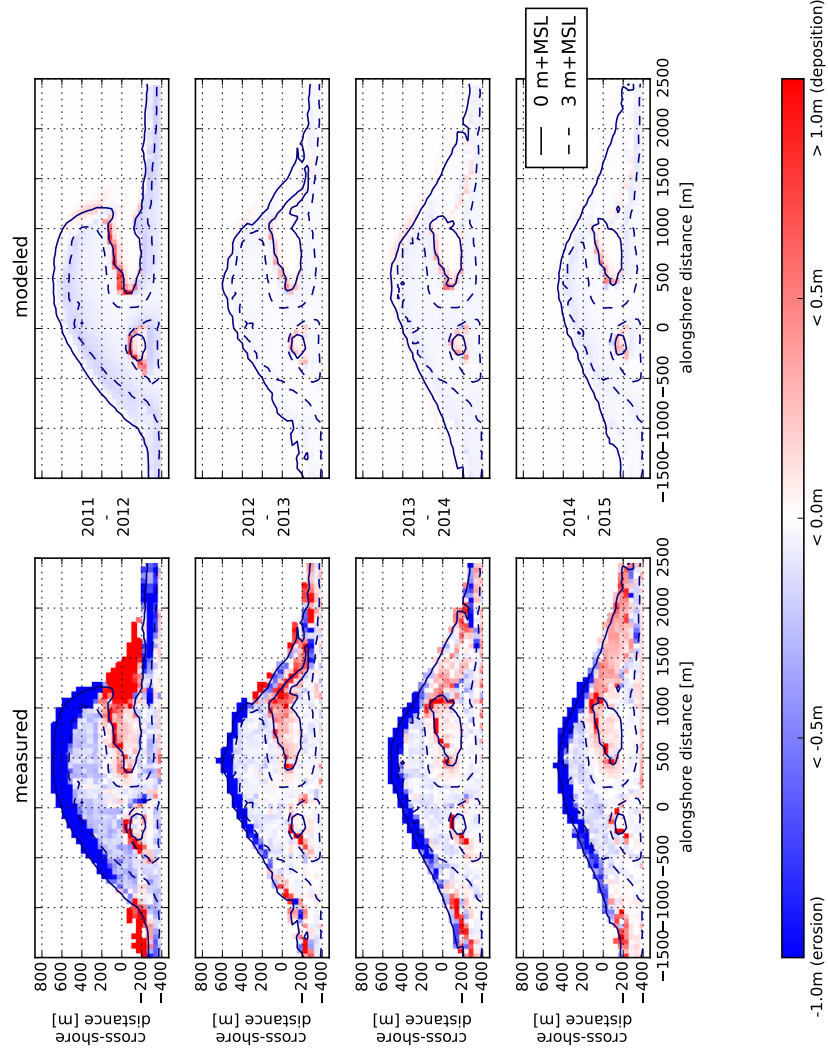


Figure 7: Measured and modeled yearly sedimentation and erosion above 0 m+MSL. Model results only include aeolian sediment transport as hydrodynamic sediment transport is not computed. Comparisons are made between the September surveys of each year.



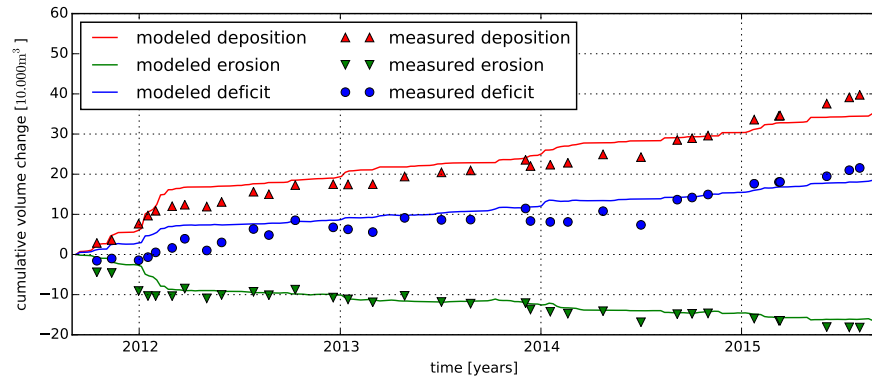


Figure 8: Measured and simulated net volume change of erosion and deposition volumes as presented in Figure ??.

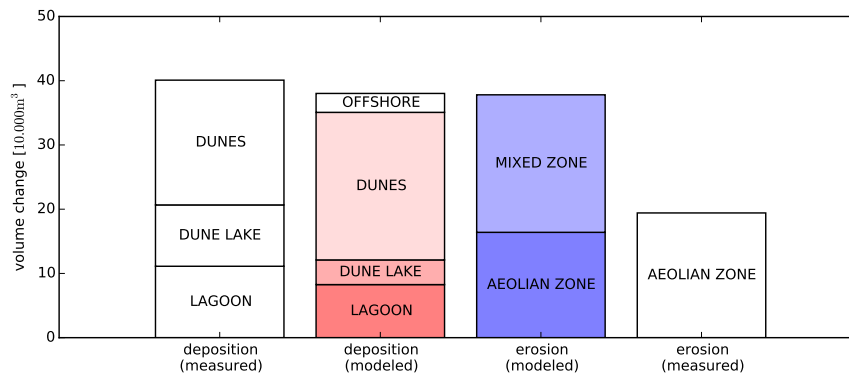


Figure 9: Total erosion and deposition volumes at the end of the simulation and measured total erosion and deposition volumes as presented in Figure ??.

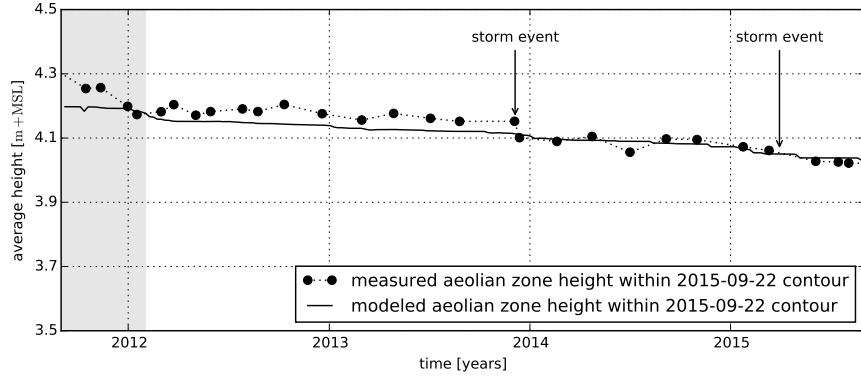


Figure 10: Measured and simulated average beach height in the aeolian zone as presented in Figure ??.

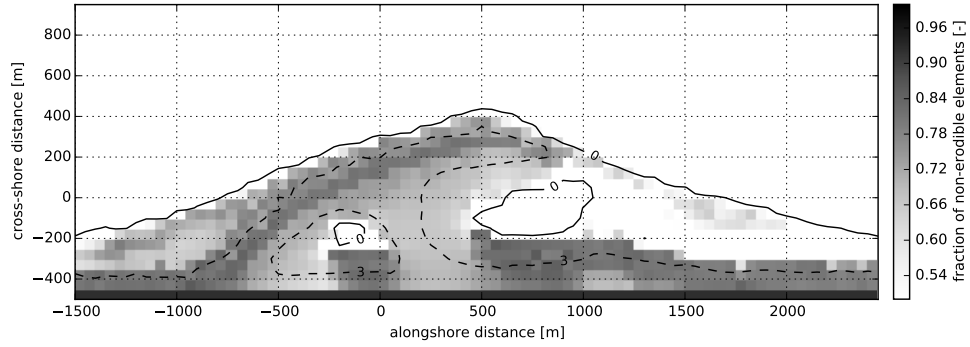


Figure 11: Simulated shell fraction in the aeolian zone at the end of the simulation.

the onshore boundary is assumed to settle in the dunes entirely. The total sediment accumulation at the end of the simulation is underestimated by 12% as the offshore sediment deposits are not included in the large scale sediment budget analysis that are used for comparison. The underestimation is unique for the last nine months of the simulation as the model overestimates the total sediment accumulation with 5% on average (Figure 8). The relative importance of the mixed zone as supplier of aeolian sediment is well captured.

The change in beach height within the most recent 3 m+MSL contour, that marks the aeolian zone, is represented by the model as the  $R^2$  value is 0.71 and the RMSE is about 4 cm or 12% of the average bed level change (Figure 10). As the change in beach height is computed within the most recent 3 m+MSL contour, the discrepancy is illustrative for the differences in spatial variability in erosion between measurements and model results. The lowering of the beach in the aeolian zone in the first half year of the simulation is particularly underestimated, while the accelerated erosion in this period is well captured in the total sediment transport. This indicates that sediment is eroded from outside the most recent 3 m+MSL contour.

The coverage of non-erodible elements  $\sigma\lambda$  [-] (Equation ??) in the aeolian zone varies between 60% and 80% at the end of the simulation (Figure 11). The coverage is high compared to the 10% – 20% shell coverage estimated to be present at the Sand Motor above 3 m+MSL based on gridded photographs.

Both the spatial and temporal variations in aeolian sediment availability are crucial for an accurate description of total sedimentation and erosion volumes as well as an accurate prediction of the aeolian sediment source and deposition areas. Figure 12 compares the total sedimentation volume according to measurements, the calibrated model and additional simulations, that are variations of the calibrated model in which spatial and/or temporal variations in the shear velocity threshold are averaged out. During these additional simulations the shear velocity threshold is not computed by the model, but space- and/or time-averaged thresholds based on the model results of the calibrated model are imposed. Negligence of the spatial variations results in a 79% underestimation of the total sedimentation volume and a relative contribution of 8% of the mixed zones. The negligence of the temporal variations results in a 46% overestimation of the total sedimentation volume and a relative contribution of 86% of the mixed zones. In addition, a simulation without limitations in sediment availability overestimates the measured total sedimentation volumes with 400%, which is comparable to the wind transport capacity following Bagnold (1937, Figure 3).

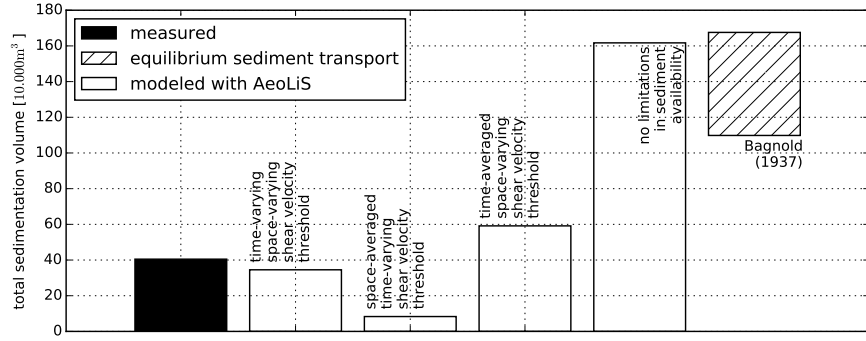


Figure 12: The influence of time-varying and space-varying shear velocity thresholds on the total sedimentation volume. The two leftmost bars depict the measured and modeled sedimentation volume as obtained from the calibrated model (Figure 9). The middle two bars depict results from two separate model simulations in which a space-averaged threshold time series or a time-averaged threshold field is imposed respectively. The threshold averages are based on the result from the calibrated model. The two rightmost columns depict a result from a separate model simulation with a constant uniform threshold based on only a constant uniform median grain size and the estimated equilibrium sediment transport following Bagnold (1937) respectively (Table 1).

## 5. Discussion

The model results show that multi-annual aeolian sediment erosion and deposition volumes, and the relative importance of the mixed zones as source of aeolian sediment are reproduced with reasonable accuracy. This suggests that indeed significant limitations in sediment availability, due to soil moisture content and beach armoring, govern aeolian sediment transport in the Sand Motor domain. A comparison with a simulation without limitation in sediment availability suggests that aeolian sediment availability in the Sand Motor domain is limited to about 25% – 35% of the wind transport capacity.

The negligence of spatial variations causes the model to underestimate the measured total sedimentation volume. The sediment supply from the relatively small mixed zone is marginalized as the imposed space-averaged shear velocity threshold is relatively high. In contrast, the negligence of temporal variations causes the model to overestimate the measured total sedimentation volume. The sediment supply from the mixed zones is increased as the effect of its periodic flooding is averaged out. At the same time, the sediment supply from the aeolian zone is decreased as the influence of beach armoring affects sediment availability from the start of the simulation rather than after the development of the beach armor layer. Therefore, the total sedimentation volume is not only overestimated, but also the importance of the mixed zones as supplier of aeolian sediment.

### 5.1. Seasonal and local variations in sedimentation and erosion

The model can reproduce multi-annual trends in sedimentation volume, which is the aim of the hindcast, but seasonal and local variations are sometimes not represented by the model. An analysis of these variations is interesting as they influence the accuracy of specific model results.

Average wind speeds tend to be elevated in December and January (Figure 2), which leads to short periods of accelerated sediment accumulation in the beginning of 2012, 2013 and 2015 that are captured well by the model. Early 2014 no accelerated sediment accumulation is measured, while the model simulation shows an increase in sediment accumulation originating from the mixed zones similar to other years.

The discrepancy early 2014 might be explained by topographic changes induced by hydrodynamic forces. On December 5th, 2013 an exceptional storm hit the Dutch coast. During this storm a significant decrease in aeolian deposits in the lagoon was observed, while deposits in the dunes and dune lake

386 increased only marginally. The assumption that the closed end of the lagoon  
387 is mainly governed by aeolian sediment transport might be violated in these  
388 exceptional conditions. At the same time, the erosion of the aeolian zone that  
389 day equaled the total erosion of the aeolian zone that year. Consequently, the  
390 total subaerial sediment volume decreased that day with about  $1 \cdot 10^4 \text{ m}^3$ ,  
391 possibly caused by hydrodynamic forces. This suggests that the simplified  
392 hydrodynamics, despite the use of a hydrodynamic mask, are a limiting factor  
393 in describing the Sand Motor's subaerial morphodynamics during extreme  
394 storms.

395 In the first months of the simulation, the total sediment accumulation  
396 is well represented, but erosion of the aeolian zone is underestimated. As  
397 beach armoring is the most important availability limitation in the aeolian  
398 zone, this suggests that the armoring rate is overestimated by the model.  
399 The armoring rate is mainly influenced by initial shell fraction of 5%, which  
400 might be overestimated. Alternatively, the initially uniform distribution of  
401 shells in the bed is not an accurate representation of reality.

402 Measured erosion and deposition rates exceed modeled erosion and depo-  
403 sition rates in the final nine months of the simulation. In this period dune  
404 growth seems to accelerate, while neither the deposition in the dune lake  
405 and lagoon did accelerate nor did the wind speed increase. The apparent  
406 acceleration is therefore solely found in the half yearly lidar measurements  
407 of the dune area (Hoonhout and de Vries, 2017) and is consequently based  
408 on a single data point. Despite the uncertainty involved in the measured ac-  
409 celeration, also precipitation rates, that were up to 70% lower in this period  
410 compared to the same period in other years, might explain the discrepancy at  
411 the end of the simulation (Jackson and Nordstrom, 1998). For the hindcast  
412 no precipitation time series are imposed as the effect on the aeolian sediment  
413 transport rate is not properly understood yet. Consequently, the calibration  
414 of the model might have resulted in an overestimated importance of beach  
415 armoring to compensate for the negligence of precipitation.

416 The distribution of the aeolian sediment deposits over the dune lake, la-  
417 goon and dunes is not represented well as deposits in the dune lake and lagoon  
418 are underestimated. Additional hydrodynamic and hydrologic processes, like  
419 wind setup and groundwater seepage, might cause the entrapment area in  
420 reality to be larger than modeled. But more importantly, the dune lake and  
421 lagoon are positioned in the lee of the Sand Motor crest with respect to the  
422 predominant southwesterly wind direction. The height difference between  
423 the Sand Motor crest and the water level in the lagoon and dune lake is

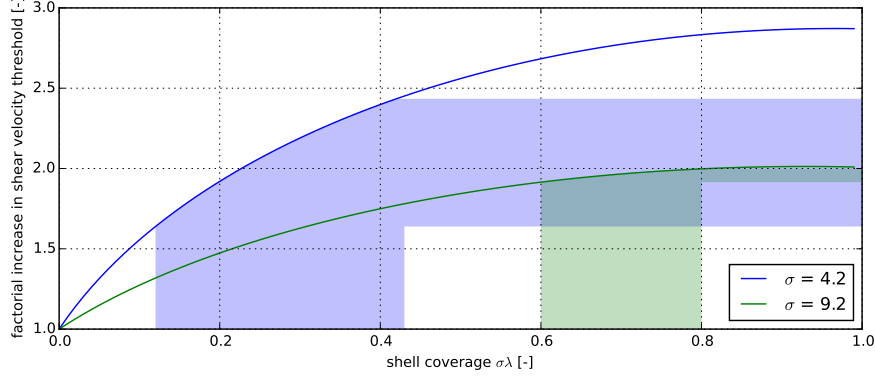


Figure 13: Relation between shear velocity threshold, shell coverage and  $\sigma$  according to Raupach et al. (1993, Equation ??). The shaded areas indicate the relevant parameter ranges from McKenna Neuman et al. (2012) (blue) and the model results (green).

several meters, which is likely to influence the local wind field significantly. The probable decrease in wind shear in the lee of the Sand Motor crest promotes deposition of aeolian sediment and likely hampers supply to the dunes. These local variations in wind shear are not included in the simulations.

### 5.2. Beach armoring, sediment availability and the shear velocity threshold

The influence of beach armoring is reflected in the model by both  $\sigma$  and the roughness density  $\lambda$  (Equation ?? and ??). The optimal value for  $\sigma$  was found to be 9.2, which is high compared to the value of 4.2 found by McKenna Neuman et al. (2012). The difference suggests that the roughness elements at the Sand Motor protrude less from the bed compared to what was found in the wind tunnel experiments. Consequently, the importance of beach armoring would be relatively low at the Sand Motor. However, the low  $\sigma$  value is largely compensated by the roughness density  $\lambda$  reflected in a shell coverage  $\sigma\lambda$  that is high compared to what was found in the wind tunnel experiments (12% – 43% on average) and what is found at the Sand Motor field site (10% – 20%). Figure 13 shows that the combination of high shell coverage and  $\sigma$  value results in a very similar increase of the shear velocity threshold compared to the wind tunnel experiments presented by McKenna Neuman et al. (2012).

The reason that the model calibration resulted in this particular value for  $\sigma$  is that the model does not differentiate between the fluid and impact

445 velocity threshold. Therefore, the roughness elements in the model affect  
 446 the initiation of sediment transport equal to the continuation of sediment  
 447 transport. The potential reduction in sediment availability increases with a  
 448 decreasing value for  $\sigma$  (if  $m = 0.5$ , Figure 13) and is implemented through an  
 449 increase in shear velocity threshold. The shear velocity threshold also affects  
 450 aeolian sediment already in transport and originating from upwind, unar-  
 451 mored beach areas, like the mixed zones. Sediments from upwind areas are  
 452 therefore partially deposited in the aeolian zone as soon a beach armor layer  
 453 develops. For low values for  $\sigma$  the local deposition of sediment from upwind  
 454 areas is already significant with low shell coverage. Low  $\sigma$  values therefore  
 455 reduce the total sediment accumulation in the dunes quickly. In order for the  
 456 model to provide reasonable total sediment transport rates, a higher value  
 457 for  $\sigma$  was found in the calibration that ultimately induces a higher shell cov-  
 458 erage. The value for  $\sigma$  therefore does not only represent a spatiotemporal  
 459 averaged emergence of roughness elements, but also a compromise between  
 460 its effect on the fluid and impact velocity threshold.

## 461 6. Conclusions

462 The Sand Motor hindcast shows that the reduction of aeolian sediment  
 463 availability due to soil moisture and beach armoring can largely explain the  
 464 low accumulation volumes in the Sand Motor domain. The AEOLiS model  
 465 has shown to be quantitatively valuable and practically applicable. The  
 466 model provides a framework for the description of complex spatiotemporal  
 467 variations in aeolian sediment availability and its relation to sediment trans-  
 468 port that has not yet been exploited in full.

469 From the hindcast the following conclusions can be drawn:

- 470 • The AEOLiS model is able to reproduce multi-annual aeolian sediment  
 471 transport rates in the Sand Motor domain in the four years after its  
 472 construction with a RMSE of  $3 \cdot 10^4 \text{ m}^3$  and  $R^2$  of 0.93 when time series  
 473 of measured and modeled total aeolian sediment transport volumes are  
 474 compared.
- 475 • The AEOLiS model is able to reproduce large scale spatial patterns in  
 476 aeolian sediment transport in the Sand Motor domain in the four years  
 477 after its construction, but underestimates the deposition in the dune  
 478 lake and lagoon.



- 479 • The AEOLIS model overestimates the total sedimentation volume with  
480 5% on average, but underestimates the total sedimentation volume with  
481 12% at the end of the simulation. The discrepancy at the end of the  
482 simulation might be caused by a particularly dry season as precipitation  
483 is not included in the simulations.
- 484 • The AEOLIS model is able to capture the seasonal variations in sed-  
485 iment transport in all years, except for early 2014 when significant  
486 morphological change is possibly related to hydrodynamic sediment  
487 transport that is not included in the simulations.
- 488 • The AEOLIS model overestimates the shell coverage, which compen-  
489 sates the high value for  $\sigma$ . The high  $\sigma$  value is a compromise between  
490 the fluid and impact threshold that are currently assumed to be equal.
- 491 • The combination of spatial and temporal variations in aeolian sediment  
492 availability, due to the combined influence of soil moisture, sediment  
493 sorting and beach armoring, and the feedback between aeolian sediment  
494 availability and transport is essential for an accurate estimate of the  
495 total sedimentation volume and the corresponding aeolian sediment  
496 source areas in the Sand Motor domain.

## 497 Acknowledgements

498 The work discussed in this paper is supported by the ERC-Advanced  
499 Grant 291206 – Nearshore Monitoring and Modeling (NEMO).

## 500 References

- 501 Aagaard, T. (2014). Sediment supply to beaches: Cross-shore sand transport  
502 on the lower shoreface. *Journal of Geophysical Research*, 119(4):913–926.  
503 doi:10.1002/2013JF003041. 2013JF003041.
- 504 Arens, S. M. (1996). Patterns of sand transport on vegetated foredunes.  
505 *Geomorphology*, 17:339–350.
- 506 Bagnold, R. (1937). The transport of sand by wind. *Geographical journal*,  
507 pages 409–438.

- 508 Barchyn, T. E., Martin, R. L., Kok, J. F., and Hugenholtz, C. H. (2014).  
509 Fundamental mismatches between measurements and models in aeolian  
510 sediment transport prediction: The role of small-scale variability. *Aeolian*  
511 *Research*, 15:245–251. doi:10.1016/j.aeolia.2014.07.002.
- 512 Bauer, B. O., Davidson-Arnott, R. G. D., Hesp, P. A., Namikas, S. L.,  
513 Ollerhead, J., and Walker, I. J. (2009). Aeolian sediment transport on  
514 a beach: Surface moisture, wind fetch, and mean transport. *Geomorphol-*  
515 *ogy*, 105:106–116. doi:10.1016/j.geomorph.2008.02.016.
- 516 Belly, P. Y. (1964). Sand movement by wind. Technical Report 1, U.S. Army  
517 Corps of Engineers CERC, Vicksburg, MS. 38 pp.
- 518 Cheng, H., Liu, C., Zou, X., Li, J., He, J., Liu, B., Wu, Y., Kang, L.,  
519 and Fang, Y. (2015). Aeolian creeping mass of different grain sizes  
520 over sand beds of varying length. *Journal of Geophysical Research*.  
521 doi:10.1002/2014JF003367. 2014JF003367.
- 522 Darke, I. and McKenna Neuman, C. (2008). Field study of beach water  
523 content as a guide to wind erosion potential. *Journal of Coastal Research*,  
524 24(5):1200–1208. doi:10.2112/00-000.1.
- 525 Davidson-Arnott, R. G. D. and Bauer, B. O. (2009). Aeolian sediment trans-  
526 port on a beach: Thresholds, intermittency, and high frequency variability.  
527 *Geomorphology*, 105:117–126. doi:10.1016/j.geomorph.2008.02.018.
- 528 Davidson-Arnott, R. G. D., Yang, Y., Ollerhead, J., Hesp, P. A., and Walker,  
529 I. J. (2008). The effects of surface moisture on aeolian sediment transport  
530 threshold and mass flux on a beach. *Earth Surface Processes and Land-*  
531 *forms*, 33(1):55–74. doi:10.1002/esp.1527.
- 532 de Vries, S., Radermacher, M., de Schipper, M., and Stive, M. (2015). Tidal  
533 dynamics in the Sand Motor lagoon. In *E-proceedings of the 36th IAHR*  
534 *World Congress*.
- 535 de Vries, S., van Thiel de Vries, J. S. M., van Rijn, L. C., Arens, S. M.,  
536 and Ranasinghe, R. (2014). Aeolian sediment transport in supply limited  
537 situations. *Aeolian Research*, 12:75–85. doi:10.1016/j.aeolia.2013.11.005.

- 538 Dupont, S., Bergametti, G., and Simoëns, S. (2014). Modeling aeolian erosion  
539 in presence of vegetation. *Journal of Geophysical Research*, 119(2):168–187.  
540 doi:10.1002/2013JF002875.
- 541 Dyer, K. R. (1986). *Coastal and estuarine sediment dynamics*. Wiley, Chich-  
542 ester.
- 543 Edwards, B. L. and Namikas, S. L. (2009). Small-scale variability in sur-  
544 face moisture on a fine-grained beach: implications for modeling ae-  
545olian transport. *Earth Surface Processes and Landforms*, 34:1333–1338.  
546 doi:10.1002/esp.1817.
- 547 Gillette, D. A. and Stockton, P. H. (1989). The effect of nonerodible particles  
548 on wind erosion of erodible surfaces. *Journal of Geophysical Research:*  
549 *Atmospheres*, 94(D10):12885–12893. doi:10.1029/JD094iD10p12885.
- 550 Gillies, J. A., Nickling, W. G., and King, J. (2006). Aeolian sediment  
551 transport through large patches of roughness in the atmospheric iner-  
552 tial sublayer. *Journal of Geophysical Research: Earth Surface*, 111(F2).  
553 doi:10.1029/2005JF000434. F02006.
- 554 Hoonhout, B. M. and de Vries, S. (2016). A process-based model for aeolian  
555 sediment transport and spatiotemporal varying sediment availability. *Jour-  
556 nal of Geophysical Research: Earth Surface*. doi:10.1002/2015JF003692.  
557 2015JF003692.
- 558 Hoonhout, B. M. and de Vries, S. (2017). Aeolian sediment supply at a mega  
559 nourishment. *Coastal Engineering*. doi:10.1016/j.coastaleng.2017.03.001.  
560 Submitted.
- 561 Horikawa, K., Hotta, S., Kubota, S., and Katori, S. (1983). On the sand  
562 transport rate by wind on a beach. *Coastal Engineering in Japan*, 26:101–  
563 120.
- 564 Hotta, S., Kubota, S., Katori, S., and Horikawa, K. (1984). Sand transport  
565 by wind on a wet sand beach. In *Proceedings of the 19th Conference on*  
566 *Coastal Engineering*, pages 1264–1281, Houston, TX. ASCE.
- 567 Howard, A. D. (1977). Effect of slope on the threshold of mo-  
568 tion and its application to orientation of wind ripples. *Geolog-  
569 ical Society of America Bulletin*, 88(6):853–856. doi:10.1130/0016-  
570 7606(1977)88;853:EOSOTT;2.0.CO;2.

- 571 Jackson, D. W. T. and Cooper, J. A. G. (1999). Beach fetch distance and ae-  
 572olian sediment transport. *Sedimentology*, 46:517–522. doi:10.1046/j.1365-  
 5733091.1999.00228.x.
- 574 Jackson, N. L. and Nordstrom, K. F. (1998). Aeolian transport of sediment  
 575on a beach during and after rainfall, wildwood, nj, usa. *Geomorphology*,  
 57622(2):151–157. doi:10.1016/S0169-555X(97)00065-2.
- 577 Johnson, J. W. (1965). Sand movement on coastal dunes. Technical Report  
 578570, Symp. 3, Paper no. 75, U.S. Department of Agriculture, Washington.  
 579pp 747-755.
- 580 Kawamura, R. (1951). Study of sand movement by wind. Technical Re-  
 581port HEL-2-8, Hydraulics Engineering Laboratory, Univeristy of Califor-  
 582nia, Berkeley.
- 583 King, J., Nickling, W. G., and Gillies, J. A. (2005). Representation of vege-  
 584tation and other nonerodible elements in aeolian shear stress partitioning  
 585models for predicting transport threshold. *Journal of Geophysical Re-*  
 586*search*, 110(F4). doi:10.1029/2004JF000281. F04015.
- 587 Lancaster, N. and Baas, A. (1998). Influence of vegetation cover on sand  
 588transport by wind: field studies at owens lake, california. *Earth Surface*  
 589*Processes and Landforms*, 23(1):69–82.
- 590 Lettau, K. and Lettau, H. (1978). *Exploring the World's Driest Climate.*,  
 591chapter Experimental and micrometeorological field studies of dune mi-  
 592gration., pages 110–147. University of Wisconsin - Madison. IES Report  
 593101,.
- 594 Li, J., Okin, G. S., Herrick, J. E., Belnap, J., Miller, M. E., Vest, K., and  
 595Draut, A. E. (2013). Evaluation of a new model of aeolian transport in the  
 596presence of vegetation. *Journal of Geophysical Research*, 118(1):288–306.  
 597doi:10.1002/jgrf.20040.
- 598 Lynch, K., Jackson, D. W. T., and Cooper, J. A. G. (2008). Aeolian fetch  
 599distance and secondary airflow effects: the influence of micro-scale vari-  
 600ables on meso-scale foredune development. *Earth Surface Processes and*  
 601*Landforms*, 33(7):991–1005. doi:10.1002/esp.1582.

- 602 McKenna Neuman, C., Li, B., and Nash, D. (2012). Micro-  
603 topographic analysis of shell pavements formed by aeolian transport in  
604 a wind tunnel simulation. *Journal of Geophysical Research*, 117(F4).  
605 doi:10.1029/2012JF002381. F04003.
- 606 McKenna Neuman, C. and Sanderson, S. (2008). Humidity control of particle  
607 emissions in aeolian systems. *Journal of Geophysical Research*, 113(F2).  
608 doi:10.1029/2007JF000780. F02S14.
- 609 Namikas, S. L., Edwards, B. L., Bitton, M. C. A., Booth, J. L., and  
610 Zhu, Y. (2010). Temporal and spatial variabilities in the surface mois-  
611 ture content of a fine-grained beach. *Geomorphology*, 114:303–310.  
612 doi:10.1016/j.geomorph.2009.07.011.
- 613 Nickling, W. G. and Ecclestone, M. (1981). The effects of soluble salts on  
614 the threshold shear velocity of fine sand. *Sedimentology*, 28:505–510.
- 615 Okin, G. S. (2008). A new model of wind erosion in the presence of vegetation.  
616 *Journal of Geophysical Research*, 113(F2). doi:10.1029/2007JF000758.  
617 F02S10.
- 618 Peckham, S. D., Hutton, E. W. H., and Norris, B. (2013). A component-based  
619 approach to integrated modeling in the geosciences: The design of CSDMS.  
620 *Computers and Geosciences*, 53:3–12. doi:10.1016/j.cageo.2012.04.002.
- 621 Raupach, M., Gillette, D., and Leys, J. (1993). The effect of roughness  
622 elements on wind erosion threshold. *Journal of Geophysical Research: At-*  
623 *mospheres*, 98(D2):3023–3029. doi:10.1029/92JD01922.
- 624 Scheidt, S., Ramsey, M., and Lancaster, N. (2010). Determining soil moisture  
625 and sediment availability at white sands dune field, new mexico, from  
626 apparent thermal inertia data. *Journal of Geophysical Research*, 115(F2).  
627 doi:10.1029/2009JF001378. F02019.
- 628 Sherman, D. J., Jackson, D. W., Namikas, S. L., and Wang, J. (1998).  
629 Wind-blown sand on beaches: an evaluation of models. *Geomorphology*,  
630 22(2):113–133. doi:10.1016/S0169-555X(97)00062-7.
- 631 Sherman, D. J. and Li, B. (2012). Predicting aeolian sand trans-  
632 port rates: a reevaluation of models. *Aeolian Research*, 3(4):371–378.  
633 doi:10.1016/j.aeolia.2011.06.002.

- 634 Stive, M. J. F., de Schipper, M. A., Luijendijk, A. P., Aarninkhof, S. G. J.,  
635 van Gelder-Maas, C., van Thiel de Vries, J. S. M., de Vries, S., Henriquez,  
636 M., Marx, S., and Ranasinghe, R. (2013). A new alternative to saving our  
637 beaches from sea-level rise: the Sand Engine. *Journal of Coastal Research*,  
638 29(5):1001–1008. doi:10.2112/JCOASTRES-D-13-00070.1.
- 639 Stockdon, H. F., Holman, R. A., Howd, P. A., and Sallenger, A. H. (2006).  
640 Empirical parameterization of setup, swash, and runup. *Coastal engineer-*  
641 *ing*, 53(7):573–588. doi:10.1016/j.coastaleng.2005.12.005.
- 642 Tan, L., Zhang, W., Qu, J., Zhang, K., An, Z., and Wang, X. (2013). Aeolian  
643 sand transport over gobi with different gravel coverages under limited sand  
644 supply: a mobile wind tunnel investigation. *Aeolian Research*, 11:67–74.  
645 doi:10.1016/j.aeolia.2013.10.003.
- 646 Udo, K., Kuriyama, Y., and Jackson, D. W. T. (2008). Observations of wind-  
647 blown sand under various meteorological conditions at a beach. *Journal*  
648 *of Geophysical Research*, 113(F4). doi:10.1029/2007JF000936. F04008.
- 649 van der Wal, D. (1998). The impact of the grain-size distribution of nourish-  
650 ment sand on aeolian sand transport. *Journal of Coastal Research*, pages  
651 620–631.
- 652 Wiggs, G. F. S., Baird, A. J., and Atherton, R. J. (2004). The dynamic  
653 effects of moisture on the entrainment and transport of sand by wind.  
654 *Geomorphology*, 59:13–30. doi:10.1016/j.geomorph.2003.09.002.